Transactions on Modelling and Simulation vol 18, © 1997 WIT Press, www.witpress.com, ISSN 1743-355X

Application of the fast multipole method to the 3-D BEM analysis of electron guns

T. Nishida and K. Hayami

Department of Mathematical Engineering and Information Physics, School of Engineering, University of Tokyo
7-3-1, Hongo, Bunkyo-ku, 113 Tokyo, Japan
EMail: nishida@simplex.t.u-tokyo.ac.jp,
hayami@simplex.t.u-tokyo.ac.jp

Abstract

Although BEM enjoys the boundary only discretization, the computational work and memory requirements become prohibitive for large-scale 3-D problems due to its dense matrix formulation. The computation of n-body problems, such as in charged particle simulation, has a similar inherent difficulty. In this paper, we use the Fast Multipole Method to overcome these difficulties and apply it to the 3-D analysis of electron guns, which involves both solving BEM and n-body problems.

1 Introduction

Despite the advantage of the boundary only discretization, the conventional boundary element method (BEM) suffers a crucial computational disadvantage when applying to large scale industrial problems, particularly in three-dimensional analysis. Namely, the method requires $\mathrm{O}(N^2)$ memory and $\mathrm{O}(N^3)$ computational work, where N is the number of boundary elements.

The Fast Multipole Method (FMM)[1] is a promising technique to overcome this difficulty. The method approximates the dense matrix vector multiplication required for linear iterative solvers for BEM to a prescribed accuracy with $\mathrm{O}(N)$ memory and computational work. This is done by approximating the effect of boundary elements far from the observation point using multipole expansions and clustering the effect.

The FMM is also a powerful technique for speeding up the simulation of n-body problems governed by long-distance forces. In this paper, we will apply the FMM to the 3-D Poisson equation governing the charged particle beams in electron guns used in cathode ray tubes and microwave tubes. The problem is a combination of BEM and a many body problem for the charged particles. The solution of the problem using conventional BEM is computationally prohibitive, even on a supercomputer. We will show that the application of the FMM renders the simulation feasible even on workstations. In addition, we will introduce a new block-diagonal preconditioner suited to FMM, which further improves the convergence and computational efficiency of the linear iterative solver[3].

We will also introduce analytical integration formulas for planar elements, which are necessary for computing the nearly singular integrals occurring in the calculation of the flux near the cathode of the electron gun.

2 Boundary element formulation

2.1 Boundary integral equation

Let $\boldsymbol{x}$ be a point in a domain Ω in $\boldsymbol{R}^3$ i.e. $\boldsymbol{x} \equiv (x_1, x_2, x_3)^T \in \Omega$. The three-dimensional Poisson equation is expressed as

$$-\Delta u(\boldsymbol{x}) \equiv -\frac{\partial^2 u}{\partial x^2} - \frac{\partial^2 u}{\partial y^2} - \frac{\partial^2 u}{\partial z^2} = \frac{\rho(\boldsymbol{x})}{\varepsilon}, \quad \boldsymbol{x} \in \Omega \tag{1}$$

where $u(\boldsymbol{x})$ is the electrostatic potential, $\rho(\boldsymbol{x})$ is the charge density and ε is the dielectric constant.

The boundary condition for (1) is given by

$$\begin{aligned} u(\boldsymbol{x}) &= \bar{u}(\boldsymbol{x}), \quad \boldsymbol{x} \in \Gamma^{(D)}, \\ q(\boldsymbol{x}) &= \frac{\partial u}{\partial n}(\boldsymbol{x}) = \bar{q}(\boldsymbol{x}), \quad \boldsymbol{x} \in \Gamma^{(N)}, \end{aligned}$$

where

$$\Gamma^{(D)} + \Gamma^{(N)} = \Gamma$$

$\frac{\partial}{\partial n}$ stands for the normal derivative at $\boldsymbol{x} \in \Gamma$, so that q is the normal flux.

Let $u^*(\boldsymbol{x}, \boldsymbol{x}_s)$ be the fundamental solution obtained by substituting $\delta(\boldsymbol{x}, \boldsymbol{x}_s)$ for $\frac{\rho(\boldsymbol{x})}{\varepsilon}$ in (1), $q^*(\boldsymbol{x}, \boldsymbol{x}_s)$ its normal derivative, and $\boldsymbol{x}_s$ the observation point. Here,

$$u^*(\boldsymbol{x}, \boldsymbol{x}_s) = \frac{1}{4\pi r}, \quad q^*(\boldsymbol{x}, \boldsymbol{x}_s) = -\frac{(\boldsymbol{r}, \boldsymbol{n})}{4\pi r^3},$$

where $\boldsymbol{r} = \boldsymbol{x} - \boldsymbol{x}_s$, $r \equiv |\boldsymbol{r}|$, and $\boldsymbol{n}$ is the unit outward normal vector at $\boldsymbol{x} \in \Gamma$. Then, (1) and Gauss' theorem give rise to the boundary integral equation

$$\begin{aligned} &c(\boldsymbol{x}_s)u(\boldsymbol{x}_s) + \int_\Gamma q^*(\boldsymbol{x}, \boldsymbol{x}_s)u(\boldsymbol{x})\mathrm{d}\Gamma(\boldsymbol{x}) = \\ &\int_\Gamma u^*(\boldsymbol{x}, \boldsymbol{x}_s)q(\boldsymbol{x})\mathrm{d}\Gamma(\boldsymbol{x}) + \int_\Omega u^*(\boldsymbol{x}, \boldsymbol{x}_s)\frac{\rho(\boldsymbol{x})}{\varepsilon}\mathrm{d}\Omega(\boldsymbol{x}), \end{aligned} \tag{2}$$

where

$$c(\boldsymbol{x}_s) = \begin{cases} 1, & \boldsymbol{x}_s \in \Omega \\ \frac{\omega(\boldsymbol{x}_s)}{4\pi}, & \boldsymbol{x}_s \in \Gamma \\ 0, & \text{otherwise.} \end{cases} \tag{3}$$

and $\omega(\boldsymbol{x}_s)$ is the solid angle subtending Ω at $\boldsymbol{x}_s \in \Gamma$.

2.2 Discretization by constant planar elements

Next, the boundary Γ is approximated by N constant planar elements, where $u(\boldsymbol{x})$ and $q(\boldsymbol{x})$ are assumed to be constant within each boundary element Γ_i, taking the values u_i and q_i, respectively. Let $\boldsymbol{x}_i$ be the representative point of Γ_i, e.g. its center of gravity. Then, (2) is discretized as

$$\frac{1}{2}u(\boldsymbol{x}_i) + \sum_{j=1}^{N} u_j \int_{\Gamma_j} q^*(\boldsymbol{x}, \boldsymbol{x}_i)\mathrm{d}\Gamma(\boldsymbol{x}) =$$

$$\sum_{j=1}^{N} q_j \int_{\Gamma_j} u^*(\boldsymbol{x}, \boldsymbol{x}_i)\mathrm{d}\Gamma(\boldsymbol{x}) + \int_{\Omega} u^*(\boldsymbol{x}, \boldsymbol{x}_i)\frac{\rho(\boldsymbol{x})}{\varepsilon}\mathrm{d}\Omega(\boldsymbol{x}), \quad (i = 1, \ldots, N). \tag{4}$$

Denoting

$$h_{ij} = \int_{\Gamma_j} q^*(\boldsymbol{x}, \boldsymbol{x}_i)\mathrm{d}\Gamma + \frac{1}{2}\delta_{ij}, \quad g_{ij} = \int_{\Gamma_j} u^*(\boldsymbol{x}, \boldsymbol{x}_i)\mathrm{d}\Gamma,$$

$$f_i = \int_{\Omega} u^*(\boldsymbol{x}, \boldsymbol{x}_i)\frac{\rho(\boldsymbol{x})}{\varepsilon}\mathrm{d}\Omega(\boldsymbol{x}),$$

$$\boldsymbol{u} = (u_1, u_2, \ldots, u_n)^T, \quad \boldsymbol{q} = (q_1, q_2, \ldots, q_n)^T \quad \boldsymbol{f} = (f_1, \ldots, f_n)^T,$$

where δ_{ij} is the Kronecker's delta, we obtain

$$\begin{pmatrix} H_{11} & H_{12} \\ H_{21} & H_{22} \end{pmatrix} \begin{pmatrix} \bar{\boldsymbol{u}}_1 \\ \boldsymbol{u}_2 \end{pmatrix} = \begin{pmatrix} G_{11} & G_{12} \\ G_{21} & G_{22} \end{pmatrix} \begin{pmatrix} \boldsymbol{q}_1 \\ \bar{\boldsymbol{q}}_2 \end{pmatrix} + \boldsymbol{f},$$

where $\bar{\boldsymbol{u}}_1$, $\bar{\boldsymbol{q}}_2$ are the prescribed boundary values and H_{ij}, $G_{ij}(i = 1, 2)$ are submatrices.

Then, the known vector $\bar{\boldsymbol{u}}_1$ is exchanged for the unknown vector $\boldsymbol{q}_1$ to give the following system of linear equations:

$$\begin{pmatrix} G_{11} & -H_{12} \\ G_{21} & -H_{22} \end{pmatrix} \begin{pmatrix} \boldsymbol{q}_1 \\ \boldsymbol{u}_2 \end{pmatrix} = \begin{pmatrix} H_{11} & -G_{12} \\ H_{21} & -G_{22} \end{pmatrix} \begin{pmatrix} \bar{\boldsymbol{u}}_1 \\ \bar{\boldsymbol{q}}_2 \end{pmatrix} + \boldsymbol{f}, \tag{5}$$

or

$$A\boldsymbol{x} = \boldsymbol{b}, \tag{6}$$

where matrix A is nonsymmetric and dense.

Once the unknowns on the boundary are determined, the flux at an interior point can be calculated by

$$\frac{\partial}{\partial \boldsymbol{x}_i} u(\boldsymbol{x}_i) = -\sum_{j=1}^{N} u_j \int_{\Gamma_j} \frac{\partial}{\partial \boldsymbol{x}_i} q^*(\boldsymbol{x}, \boldsymbol{x}_i) \mathrm{d}\Gamma(\boldsymbol{x})$$

$$+\sum_{j=1}^{N} q_j \int_{\Gamma_j} \frac{\partial}{\partial \boldsymbol{x}_i} u^*(\boldsymbol{x}, \boldsymbol{x}_i) \mathrm{d}\Gamma(\boldsymbol{x}) + \int_{\Omega} u^*(\boldsymbol{x}, \boldsymbol{x}_i) \frac{\rho(\boldsymbol{x})}{\varepsilon} \mathrm{d}\Omega(\boldsymbol{x}). \qquad (7)$$

3. FMM and preconditioning for BEM

In the standard boundary element method, (6) is solved using LU-decomposition, requiring $\mathrm{O}(N^3)$ computational work and $\mathrm{O}(N^2)$ memory. If we use iterative methods such as GMRES[4] for the nonsymmetric system of linear equations, the computational work is reduced to $\mathrm{O}(MN^2)$ where M is the number of iteration, but $\mathrm{O}(N^2)$ memory is still required. Hence, we will consider reducing the computational work and memory using the Fast Multipole Method(FMM). The details of the FMM algorithm is referred to [1]. In this paper, we use the adaptive version of the FMM to form the multipole and local expansions.

3.1 Clustering

The most time-consuming part of iterative methods for the solution of systems of linear equations is the matrix-vector multiplication in each iteration. The inner product between the i-th row of matrix A and the iteration vector $(\tilde{\boldsymbol{u}}_2^T, \tilde{\boldsymbol{q}}_1^T)^T$ corresponding to the solution vector $(\boldsymbol{u}_2^T, \boldsymbol{q}_1^T)^T$ is given by

$$\sum_{\Gamma_j \in \Gamma_1^{(D)}} \tilde{q}_j \int_{\Gamma_j} u^*(\boldsymbol{x}, \boldsymbol{x}_i) \mathrm{d}\Gamma - \sum_{\Gamma_j \in \Gamma_2^{(N)}} \tilde{u}_j \int_{\Gamma_j} q^*(\boldsymbol{x}, \boldsymbol{x}_i) \mathrm{d}\Gamma, \qquad (8)$$

where $\tilde{u}_j$ and $\tilde{q}_j$ are the elements of the iteration vector.

Now consider dividing the field with respect to the distance from the observation point $\boldsymbol{x}_i$, into the near field and the far field. A member $\boldsymbol{x}$ of the far field satisfies the condition

$$|\boldsymbol{x}_i - C_c| > 2|\boldsymbol{x} - C_c|, \qquad (9)$$

where C_c is the center of cluster. For the boundary elements belonging to the near field, (8) is calculated element-wise as usual.

For the elements in the far field, a hierarchy of domains containing clusters of boundary elements are constructed. Then, u^* and q^* in (8) are expressed in multipole expansions around C_c using spherical harmonics, which is given by associated Legendre polynomials. Then, the first term in

(8) including u^* is expanded as

$$\begin{aligned}\tilde{q}_j \int_{\Gamma_j} \frac{1}{|\boldsymbol{x}_i - \boldsymbol{x}|} \mathrm{d}\Gamma(\boldsymbol{x}) &= \tilde{q}_j \int_{\Gamma_j} \frac{1}{|(\boldsymbol{x}_i - \mathrm{C_c}) - (\boldsymbol{x} - \mathrm{C_c})|} \mathrm{d}\Gamma(\boldsymbol{x}) \\ &\simeq \sum_{n=0}^{p} \sum_{m=-n}^{n} \frac{M_n^m}{|\boldsymbol{x}_i - \mathrm{C_c}|^{n+1}} \cdot Y_n^m(\theta, \phi), \qquad (10)\end{aligned}$$

where

$$M_n^m = \tilde{q}_j \int_{\Gamma_j} |\boldsymbol{x} - \mathrm{C_c}|^n \cdot Y_n^{-m}(\alpha, \beta) \mathrm{d}\Gamma(\boldsymbol{x}), \qquad (11)$$

and Y_n^m is the spherical harmonic function, and we have truncated the expansion at $n = p$. $(|\boldsymbol{x} - \mathrm{C_c}|, \alpha, \beta)$ and $(|\boldsymbol{x}_i - \mathrm{C_c}|, \theta, \rho)$ are the polar coordinates centered at C_c of $\boldsymbol{x}$ on Γ_j and the observation point $\boldsymbol{x}_i$, respectively.

Similarly, the second term in (8) including q^* can be expanded as

$$\tilde{u}_j \int_{\Gamma} \nabla \left(\frac{1}{|\boldsymbol{x}_i - \boldsymbol{x}|} \right) \cdot \boldsymbol{n} \mathrm{d}\Gamma(\boldsymbol{x}) \simeq \sum_{n=0}^{p} \sum_{m=-n}^{n} \frac{M_n^m}{|\boldsymbol{x}_i - \mathrm{C_c}|^{n+1}} \cdot Y_n^m(\theta, \phi), \qquad (12)$$

where

$$M_n^m = \tilde{u}_j \int_{\Gamma_j} \nabla(|\boldsymbol{x} - \mathrm{C_c}|^n \cdot Y_n^{-m}(\alpha, \beta)) \cdot \boldsymbol{n} \mathrm{d}\Gamma(\boldsymbol{x}) \qquad (13)$$

and $\nabla(|\boldsymbol{x} - \mathrm{C_c}|^n \cdot Y_n^{-m}(\alpha, \beta)) \cdot \boldsymbol{n}$ can be expressed as

$$\begin{aligned}&\nabla(r^n \cdot Y_n^{-m}(\alpha, \beta)) \cdot \boldsymbol{n} = \\ &\quad \left[n \cdot \frac{(\boldsymbol{r}, \boldsymbol{n})}{r} \cdot Y_n^{-m}(\alpha, \beta) + \left\{ \frac{\cos\alpha}{\sin\alpha} \frac{(\boldsymbol{r}, \boldsymbol{n})}{r} - \frac{n_z}{\sin\alpha} \right\} \cdot Y'^{-m}_{n}(\alpha, \beta) \right. \\ &\quad \left. + \mathrm{i}m \frac{n_x \sin\beta - n_y \cos\beta}{\sin\alpha} \cdot Y_n^{-m}(\alpha, \beta) \right] r^{n-1}.\end{aligned}$$

Next, the coefficients M_n^m of the multipole expansions (11) or (13) can be added up for the τ elements around the same center of cluster C_c by superposition, as $O_n^m = \sum_\tau M_n^m$. Further, clusters can be merged to form larger clusters, by using the translation of multipole expansions[1]. As a result, computational work and memory required for evaluating (8) can be reduced, since O_n^m can be shared among differed $\boldsymbol{x}_i$'s.

A multipole expansion due to a cluster of elements which satisfies (9) can be converted to a local expansion about $\boldsymbol{x}_i$. This enables the efficient computation of the effect of a cluster of elements on another cluster.

The local expansion can be obtained from multipole expansions by replacing $|\boldsymbol{x}_i - \mathrm{C_c}|$ by $|\boldsymbol{x} - \mathrm{C_c}|$ in (10), (11) and (12), (13).

3.2 Preconditioners

Next, we will consider preconditioners for reducing the number of iterations for the iterative linear solver. That is, a preconditioner M which approximates the original matrix A is chosen, and the iterative method is applied to the preconditioned system

$$M^{-1}A\boldsymbol{x} = M^{-1}\boldsymbol{b}.$$

We will make use of the diagonal of the matrix A and also the components near the diagonal as the preconditioner as follows:

(1) Diagonal scaling Take the main diagonal of A as M: $M \equiv (a_{ii})$.

(2) Block diagonal scaling Here, we will propose a new preconditioner which we will call block diagonal scaling. First of all, we compute all the interactions between the boundary elements inside each cluster or domain of the lowest level, forming submatrices. Next, these submatrices are arranged diagonally to form the preconditioning matrix M. This preconditioner corresponds to the near field effect.

3.3 Numerical result

We will take the following simple three-dimensional example of an interior mixed boundary problem for the Laplace equation to demonstrate the effect of FMM and preconditioning on BEM.

$$\begin{aligned}
\Delta u &= 0 \quad \text{in} \quad \Omega \equiv \{\boldsymbol{x} | 0 < x, y, z < 1\}, \\
u(\boldsymbol{x}) &= \begin{cases} 10, & x = 0 \\ 0, & x = 1 \end{cases}, \quad \boldsymbol{x} \in \Gamma^{(D)}, \\
q(\boldsymbol{x}) &= 0, \quad 0 < x < 1, \quad \boldsymbol{x} \in \Gamma^{(N)}.
\end{aligned}$$

The boundary of the cube Ω was discretized into constant triangular boundary elements.

The problem was solved using LU-Decomposition, GMRES with diagonal scaling (diagonal GMRES), GMRES with the FMM (GMRES + FMM), GMRES with the FMM and diagonal scaling (diagonal GMRES + FMM), and GMRES with the FMM and block diagonal scaling, as shown in Fig. 1. The iterations were done until the relative residual became less than 10^{-5}. The multipole expansion for the FMM was truncated at $p = 6$. The main memory of the workstation used was 112 Mbyte.

Fig. 1 compares the CPU time (seconds) for the different methods as the number of boundary elements is increased. It was virtually impossible for the LU-decomposition and GMRES without the FMM to solve problems with number of elements more than 4000 due to the limitation of the main memory, whereas GMRES + FMM could solve problems with more than 30000 elements. If the CPU time for the diagonal GMRES is extrapolated in Fig. 1, we may estimate that diagonal GMRES + FMM will be faster than diagonal GMRES when the number of elements is larger than 20000.

As for the effect of preconditioning, the block diagonal scaling reduces the CPU time to a quarter compared to the unpreconditioned GMRES + FMM, and is considerably faster than the simple diagonal scaling.

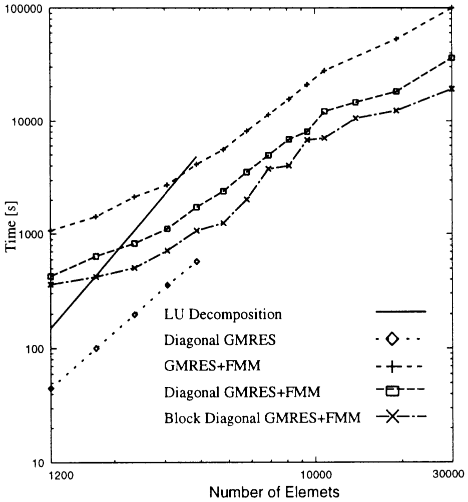

Figure 1: The effect of FMM and preconditioning.

4. Analytical integration formulae

In order to calculate the integrals appearing in equation (4) and (7) accurately when the observation point is near the boundary, we have used the following analytical integration formulae for constant planar elements. The formulae are derived using polar coordinates in the following way.

First, some variables as shown in Fig. 2 are defined, using simple coordinate transformations. Consider the influence of the element Γ_j on $\boldsymbol{x}_i$. The triangular element Γ_j is divided into $\triangle\tilde{\boldsymbol{x}}_i\boldsymbol{us}$, $\triangle\tilde{\boldsymbol{x}}_i\boldsymbol{tu}$ and $\triangle\tilde{\boldsymbol{x}}_i\boldsymbol{ts}$, where $\tilde{\boldsymbol{x}}_i$ is the foot of the perpendicular from $\boldsymbol{x}_i$ to the plane including the element Γ_j. As a result, the influence from the element Γ_j can be calculated as

$$\int_{\Gamma_j} \cdot \, \mathrm{d}\Gamma = \int_{\triangle\tilde{\boldsymbol{x}}_i\boldsymbol{us}} \cdot \, \mathrm{d}\Gamma + \int_{\triangle\tilde{\boldsymbol{x}}_i\boldsymbol{tu}} \cdot \, \mathrm{d}\Gamma - \int_{\triangle\tilde{\boldsymbol{x}}_i\boldsymbol{ts}} \cdot \, \mathrm{d}\Gamma.$$

Next, we will show how to integrate over the triangle $\triangle\tilde{\boldsymbol{x}}_i\boldsymbol{ts}$.

4.1 Integration of u^* and q^*

Define r and $\rho(\theta)$ as follows: $r = \sqrt{\rho^2 + d^2}$, $\rho(\theta) = h/\cos(\theta)$. Then, the boundary integrals of (4) can be expressed as

$$\int u^* \mathrm{d}\Gamma \;=\; \int \frac{1}{r}\mathrm{d}\Gamma = \int \mathrm{d}\theta \int \frac{\rho}{r}\mathrm{d}\rho, \qquad (14)$$

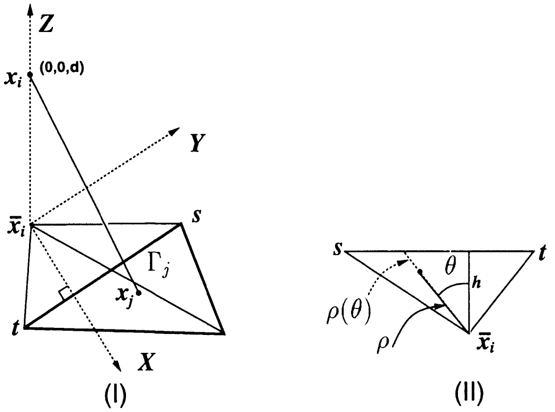

Figure 2: Variables for analytical integration.

$$\int q^* \mathrm{d}\Gamma \;=\; \int \frac{(\boldsymbol{n},\boldsymbol{r})}{r^3}\mathrm{d}\Gamma = \int \mathrm{d}\theta \int \frac{d\rho}{r^3}\mathrm{d}\rho. \qquad (15)$$

where d is the distance between $\boldsymbol{x}_i$ and Γ_j. Then, the analytic formulae for (14) and (15) are given by

$$\int \frac{1}{r}\mathrm{d}\Gamma = h\log\left|\frac{h\sin\theta+\sqrt{h^2+d^2\cos^2\theta}}{\cos\theta}\right| + d\sin^{-1}\frac{d\sin\theta}{\sqrt{h^2+d^2}} - d\theta, \qquad (16)$$

$$\int \frac{(\boldsymbol{n},\boldsymbol{r})}{r^3}\mathrm{d}\Gamma = \sin^{-1}\frac{d\sin\theta}{\sqrt{h^2+d^2}} - \theta, \qquad (17)$$

respectively.

4.2 Integration for the flux

The (x,y,z) components of the flux integral $\int \frac{\partial u^*}{\partial \mathbf{x}_i}\mathrm{d}\Gamma = \int \frac{\boldsymbol{r}}{r^3}\mathrm{d}\Gamma$ appearing in (7) are

$$\left(\log\left|\frac{h+\sqrt{h^2+d^2\cos^2\theta}}{d\cos\theta}\right|\cdot\sin\theta - \log\left|\frac{h\sin\theta+\sqrt{h^2+d^2\cos^2\theta}}{\cos\theta}\right|,\right.$$
$$\left. -\log\left|\frac{h+\sqrt{h^2+d^2\cos^2\theta}}{d\cos\theta}\right|\cdot\cos\theta, -\sin^{-1}\frac{d\sin\theta}{\sqrt{h^2+d^2}} + \theta\right),$$

respectively.

Similarly, the components for $\int \frac{\partial q^*}{\partial \mathbf{x}_i}\mathrm{d}\Gamma = \int\{\frac{\boldsymbol{n}}{r^3} - \frac{3(\boldsymbol{r},\boldsymbol{n})\boldsymbol{r}}{r^5}\}\mathrm{d}\Gamma$ are

$$\frac{1}{\sqrt{h^2+d^2\cos^2\theta}}\left(-\frac{h^3\sin\theta}{d(h^2+d^2)}, \frac{h\cos\theta}{d}, -\frac{h^2\sin\theta}{h^2+d^2}\right),$$

respectively.

5. Application to simulation of electron guns

5.1 The algorithm

We will apply the FMM reinforced BEM to the simulation of electron guns. The electron gun is the device used in cathode ray tubes or microwave tubes. The electrons emitted from the cathode are accelerated by the electron lens formed by the anodes. The electrons also interact with each other, which can be modelled by a Poisson equation.

When designing the electron gun, it is important to predict the current-voltage characteristics and the focusing characteristics of the electron beams. The numerical simulation of the electron gun is done as follows [2].

1. Solve the Laplace equation (1) for the electrostatic potential with $\rho(\boldsymbol{x}) = 0$.
2. Set a virtual cathode which is a surface sufficiently near and parallel to the cathode. Discretize the virtual cathode into a mesh.
3. Calculate the potential at each mesh point of the virtual cathode.
4. Calculate the current density at the cathode using the potential difference between the cathode and the virtual cathode, according to Child-Langmuir's law.
5. Based on 4, assign a charge and velocity to each representative particle to be emitted from the cathode. Then, compute the trajectory of each charged particle under the electrostatic field.
6. Calculate the charge density $\rho(\boldsymbol{x})$ due to the trajectories of the electron beams.
7. Solve the Poisson equation (1) for the new electrostatic potential and go to 3.

This process is repeated until the value of the current at the cathode converges. Child-Langmuir's law used in 4 is given by

$$J = k\frac{V^{3/2}}{d^2}, \qquad k = \frac{4\varepsilon}{9}\sqrt{\frac{2e}{m}} = 2.33 \times 10^{-6},$$

where J is the electric current density, V is the difference between the voltage of the virtual cathode and the cathode, d is the distance between the cathode and the virtual cathode, e and m is the charge and mass of the electron, respectively. In the simulation, the charge density $\rho(\boldsymbol{x})$ is modelled as a collection of point charges q_i at $\boldsymbol{x}_i$, i.e., $\rho(\boldsymbol{x}) = \sum_i q_i \delta(\boldsymbol{x}, \boldsymbol{x}_i)$ where $\delta(\boldsymbol{x}, \boldsymbol{x}_i)$ is the delta function, and the position $\boldsymbol{x}_i$ is chosen as a point in between successive positions of the charged particle, i.e.,

$$\boldsymbol{x}_i = (1 - \lambda)\boldsymbol{x}(t + \Delta t) + \lambda \boldsymbol{x}(t).$$

The value of λ is chosen to be $1/3 \sim 1/2$.

The BEM is suited to the simulation of electron guns because it involves complex 3-D geometry and requires accurate flux calculations for the trajectories of the charged particles. However, the modelling of the complex geometry of the full electron gun requires an order of 10^4 boundary elements, which is not feasible with conventional BEM. Therefore, we have applied the FMM to BEM in this application. Numerical experiment results of the electron gun simulation will be presented at the conference.

Acknowledgements

The authors would like to thank Dr. S. Doi, Mr. Y. Yanai and Mr. M. Takahashi of NEC Corporation, Japan for their cooperation concerning the electron gun simulation.

References

[1] Greengard, L., *The Rapid Evaluation of Potential Fields in Particle Systems*, The MIT Press, Cambridge, 1988.

[2] MacGregor, D., M., Computer-aided design of color picture tubes with a three dimensional model, *IEEE Transactions on Consumer Electronics*, Vol. CE-29, No.3, pp. 318-325, August 1983.

[3] Nishida, T. and Hayami, K., A fast multipole method for the three-dimensional Poisson equation arising in the electron gun simulation, *Proceedings of the 17th Symposium on Computational Electrical and Electronic Engineering*, Japan Simulation Society, Tokyo, pp. 185-188, 1996 (in Japanese).

[4] Saad, Y. and Schults, M. H., A Generalized minimal residual algorithm for solving nonsymmetric linear systems, *SIAM Journal on Scientific and Statistical Computing*, Vol. 7, No. 3, pp. 856-869, 1986.